Supporting Information Appendix for

What Controls the Chemical Mixing State of Submicron Sea Spray Aerosols? The Role of Jet versus Film Drops

Authors: Xiaofei Wang, Grant B. Deane, Kathryn A. Moore, Olivia S. Ryder, M. Dale Stokes, Charlotte M. Beall, Douglas B. Collins, Mitchell V. Santander, Susannah M. Burrows, Camille M. Sultana and Kimberly A. Prather

This PDF file includes:

SI Methods

SI Figures

SI References

SI METHODS

A number of methods were used in this study to produce specific types of sea spray aerosols (SSA). The general experimental set-up for the characterization of these SSA particles is shown in *SI Appendix* Fig. S1. The air source used particle free air, which was produced from a zero air generator and then filtered by a high efficiency particulate air (HEPA) filter. All SSA particles were dried by silica diffusion dryers before conducting any aerosol measurements, except when SSA were collected using a MOUDI.

Natural seawater collection and synthetic seawater preparation. All natural seawater used in this study was collected ~ 200 m offshore from Scripps Pier (La Jolla, CA; 32°51´56.8"N: 117° 15´38.48"W), coarsely filtered through sand and then by a 20 μm filter, except for the MART experiment, which used a 50 μm filter to retain phytoplankton. The pump inlet at the pier is approximately 5 meters below the seawater surface. The collected seawater was used in the experiment within hours of collection. The synthetic seawater used in this study was prepared using ultrapure water (18 MΩ) and ACS grade salts with the following mass fractions: NaCl 2.398%; $MgCl_2$ 0.5029%; Na_2SO_4 0.401%; $CaCl_2$ 0.114%; KCl 0.0699%; $NaHCO_3$ 0.0172%; KBr 0.01%; H_3BO_3 0.00254% and $SrCl_2$ 0.00143%.

Sub-100 μm bubble generation from seawater electrolysis. Electrolysis of seawater was used to produce sub-100 μm bubbles with a lognormal size distribution centered at 22 μm radius (*SI Appendix* Fig. S2A). The size distribution of the bubbles was measured using high-speed streak photography. More than 300 bubbles were measured to obtain the size distribution. The length of bubble streaks measured over a known light integration time allow for the calculation of bubble velocity, which was then converted into bubble radius. Special care was taken to ensure that collective buoyancy and boundary flow effects did not bias the velocity measurements. A voltage

source was used to drive a 21 mA current between a Nichrome cathode and copper anode. The reduction of water to H_2 (g) at the cathode nucleated small bubbles of hydrogen gas on the surface of the Nichrome wire. At the anode, Cu (s), in the presence of Cl^- (aq), was likely oxidized both to Cu^{2+} and $CuCl_2^-$.

The reaction was conducted in a cylindrical tank (*SI Appendix* Fig. S1B) filled with approximately 8 L of seawater, and the headspace flushed with particle-free air to convey SSA produced in the chamber to particle sizing and chemical characterization instruments. The cathode consisted of 0.5 m of 200 µm diameter Nichrome wire wrapped into a ~1.5 cm diameter coil. This was immersed directly in the seawater in the center of the tank, and the hydrogen bubbles produced during electrolysis, which were approximately 22 µm in radius (see Fig. 1, inset), would rise to the surface of the tank and burst, generating jet drops. Bubbles of such small sizes burst almost immediately (the lifetime for a 20 µm bubble is less than about several milliseconds) once they reach the seawater surface (1). Thus, it is unlikely that sub-100 µm bubbles would coalesce and form larger bubbles, which was also confirmed by visual observation during the experiment.

The aerosol collection inlet consisted of a plastic funnel with the wider end just above the surface of the water, attached to 3/8" SS tubing that passed through the lid of the tank. This cone was used to generate air flow turbulence near the surface of the water and thereby increase collection efficiency of the primarily supermicron aerosols produced through this method. The anode consisted of insulated copper wire that was stripped at one end and inserted into a large glass test tube, with a sponge filling the open end to serve as a salt bridge. This setup was used to keep the anode reaction products isolated from SSA production in the main chamber of the tank. The calculation of SSA particle flux from bubble flux is shown in the following section.

Calculation of SSA particle flux from electrolysis bubble flux. Using the measured hydrogen production rate (~ 2.61×10^{-9} m^3/s) and the size distribution of the hydrogen bubbles, the bubble flux is estimated to be 1.33×10^4 bubbles/s. The total number concentration of SSA (705 particles/mL) is found by integrating the area under the SSA size distribution. Multiplying the SSA concentration by the air flow rate through the electrolysis chamber (26.67 mL/s) yields the SSA flux: 1.88×10^4 particles/s. Dividing these fluxes, we can see that each bubble produces on average ~1.4 SSA drops, which may include one primary jet drop and 0.4 (in average) other types of jet drops, such as second or satellite jet drops.

Previous studies show that bursting a bubble of radius 0.3 mm and larger can produce up to 7 jet drops (2), which is significantly larger than our stated value. We note that we are not alone in observing that bubbles of the sub-50 μm scale do not produce as many jet drops as their larger counterparts. Lee et al. (2) used an x-ray imaging technique to visualize jet drop formation from bubbles in the size range that we are concerned with – less than 50 μm radius. They found that only 0-3 jet drops are formed for bubbles of this scale. For example, Lee et al. show that bursting a 26.5 um bubble in fresh water produces 3 jet drops. Although Lee et al. did not study bursting seawater bubbles, bursting freshwater bubbles should be a good proxy since seawater and freshwater have similar viscosity and surface tension. As stated above, our electrolysis experiment shows that we collected on average 1.4 jet drops from a distribution of bubbles with a number density peak at 22 um, which is generally consistent with the range of values observed by Lee et al.

Sub-100 μm bubble generation from bubble nucleation. A sub-100 μm ultrafine bubble generator or "nucleation bubbler" was developed to produce bubbles with radii less than 20 μm (*SI Appendix* Fig. S2B). As shown in *SI Appendix* Fig. S1C, the nucleation bubbler consists of

two chambers. One is a chamber filled with seawater and connected to a compressed air source held at 345 kPa. An orifice with a valve connects this pressurized chamber to an unpressurized secondary chamber filled with 3 L of seawater. When the valve is opened, pressurized seawater flows through the orifice into the unpressurized chamber, where it produces numerous sub-100 μm radius bubbles due to supersaturation and effervescence (equivalent to opening a carbonated beverage). These bubbles rise to the water surface and burst. Particle-free air was injected through the headspace of the secondary chamber at 2 liters per minute (LPM). This air transferred SSA particles produced in the chamber to the particle characterization instruments.

Bubble generation using a glass frit. As shown in *SI Appendix* Fig. S1D, a glass tank was filled with ~8 L seawater. Particle-free air was sparged with a glass frit at a rate of 0.5 LPM (Pore size: 145-174 micron, Ace glass, Inc.) producing large bubbles, some of which coalesced and formed foam. A 1.5 LPM particle-free air stream was injected into the chamber headspace to transport particles to aerosol characterization instrumentation.

SSA production using a marine aerosol reference tank (MART). Approximately 2,000 L of natural seawater was drawn from La Jolla Shores Beach in the neighborhood of the SIO pier on 7/24/2016 and placed into a polycarbonate tank, illuminated with direct sunlight. Algae growth medium (f/20 concentration, Proline, Aquatic Eco-Systems, Apopka, FL) and solutions of sodium metasilicate were added to the tank to initiate a phytoplankton bloom cycle (3). Chlorophyll-a concentrations in seawater were measured fluorometrically using a Turner AquaFluor handheld unit. Once a day, ~120 L of seawater were transferred to a MART, where SSA were generated by a periodic plunging waterfall (4 seconds on followed by 10 seconds off). Details of the bubble size distribution and MART operations can be found in Stokes et al. (4). Particle-free air was introduced into the MART headspace with a flow rate of 5 LPM to transport

SSA to on-line instrumentation to measure its size and electrical mobility distributions. At the end of each experiment day, the MART seawater was transferred back to the growing plankton culture in the polycarbonate tank.

Measurement of electrical mobility distribution (EMD) of aerosol particles. The electrical mobility (Z_p) of a particle is defined by: $Z_p = \frac{neC}{3\pi\mu D_p}$, where *n* is the number of electrical charges, D_p is particle dry diameter, *e* is elemental charge, *C* is the Cunningham slip correction factor and μ is the viscosity of air. Electrical mobility distributions of charged aerosol particles were measured using a differential mobility analyzer (DMA, Model 3081, TSI Inc., MN, USA) followed by a condensational particle counter (CPC, Model 3787, TSI Inc., MN, USA) (5). This system is similar to a scanning mobility particle sizer (SMPS) system, but without a neutralizer. An impactor (50% cut-off size: ~800 nm) was placed in-line before the DMA to remove supermicron particles.

Figure 2 shows the EMDs of SSA produced during a MART phytoplankton bloom experiment and fitted log-normal modes. The fitting process was done using Igor Pro (Version 6, WaveMetrics Inc.). The only restriction on this fitting process is that the POS1 mode is set to be equal to the NEG1 mode. Note, a small fraction (~10%) of the submicron SSA particles were not charged, and we assume that these all came from film drops to keep our jet drop particle estimate conservative.

Measurement of aerosol particle size distribution. A scanning mobility particle sizer (a combination of particle charge neutralizer, DMA and CPC: Neutralizer, Model 3088; DMA, Model 3081; CPC, Model 3787, TSI Inc., MN, USA) was used to measure particle size distributions from 0.01 to 0.8 μm dry diameter. An aerodynamic particle sizer (APS, Model 3321,

TSI Inc., MN, USA) was used to measure particle size distributions from 0.5 to 20 μm dry diameter.

Measurement of SSA chemical composition. The organic composition of SSA was measured using a high-resolution aerosol mass spectrometer (HR-AMS, Aerodyne Research Inc., MA, USA). The detailed description of HR-AMS can be found in previous publications (6). Briefly, aerosol particles enter the HR-AMS and are collected on a vaporizer at a temperature of 650 °C, where non-refractory material is vaporized. Electron impact ionization (EI) coupled with a high resolution time-of-flight mass spectrometer was used to ionize and analyze the resulting gas phase species. The ion formula of peaks, such as $C_xH_yO_z$, were determined based on their accurate mass (7).

The SSA sources for HR-AMS analysis were the nucleation and frit bubbler, which were run seperately. Since bubble gas flow rate for the frit was significantly higher than that for the nucleation bubbler, the depletion of organic surfactants for the frit bubbler could potentially limit their concentration in film drop particles. However, submicron film drop particles from the frit experiments still contained a higher fraction of aliphatic rich organics than submicron jet drop particles from the nucleation bubbler. These aliphatic rich organics most likely originate from lipids, a class of surface active organics (8, 9).

Measurement of SSA ice nucleation activity. INE concentrations were measured using an automated immersion mode technique. Submicron SSA samples were collected by filtering 1 LPM of air after a cyclone size filter (cutoff size: ~ 1 μm) for 3 h through a 47 mm diameter in-line stainless steel filter holder fitted with a 0.05 μm diameter pore Nuclepore polycarbonate membrane (Whatman). A 3 μm Nuclepore membrane was added behind the sampling membrane

to avoid direct contact between the sampling filter and filter housing. Filter holders and sampling tubes were cleaned by soaking in 10% H_2O_2 for at least 60 min followed by at least three rinse cycles with deionized water (18 MΩ and 0.2 μm diameter-pore filtered) and then dried. Filters were also soaked in 10% H_2O_2 for at least 10 min in a sterile petri dish, rinsed with deionized water and then dried. After particle collection, filters were stored at -20°C until they were processed.

For transfer of particles to water, filters were placed in sterile 50 mL Falcon polypropylene tubes (Corning Life Sciences) filled with 5 mL of deionized water (18 MΩ and 0.2 μm diameter-pore filtered). Immersion freezing temperature spectra of INE were measured using 24 aliquots of 50 μL of the solution containing SSA dispensed to sterile polymerase chain reaction (PCR) trays (LS-9796, Life Science Products Inc.). Then the tray was transferred to the automated ice spectrometer.

A refrigerated bath circulator was used for cooling the trays. Loaded PCR trays were placed in two aluminum blocks which are submerged in the coolant bath cavity of a Fisher™ Isotemp™ Refrigerated Bath Circulator, covered with a plexiglass window and purged with 0.25 LPM of particle-free nitrogen. The temperature was then lowered with a cooling rate of -0.86 ^{o}C min^{-1} and measured with a thermistor imbedded at the base of a well in the sample tray. Freezing events were counted using a software-controlled camera, which monitored changes in the optical properties of water droplets during freezing. Cumulative numbers of INE, in units of #/mL of suspension water, were calculated using the formula $\ln(f)/V$, where f is the fraction of vials not frozen and V is the volume of each aliquot. Filter blanks were also measured to obtain a mean background INE spectrum.

The following equation was used to calculate 95% binomial sampling confidence intervals (10):

$$\mathrm{CI}_{95\%} = \left(\hat{p} + \frac{1.96^2}{2n} \pm 1.96 \sqrt{\left[\hat{p}(1-\hat{p}) + {1.96^2}/{4n} \right] / n} \right) / \left(1 + {1.96^2}/{n} \right),$$

where $\hat{p}$ is the fraction of vials frozen and *n* is the total number of vials.

Measurement of SSA organic volume fraction. Aerosol particles were collected on methanol-cleaned Silicon wafer chips (Ted Pella, product number 16008) using stages 6 and 7 of a rotating Micro-Orifice Uniform Deposition Impactor (MSP Nano-MOUDI II, model 125R). A Bruker Dimension Icon ScanAsyst Atomic Force Microscope was used to image particles at room temperature (~298K) and ~60% RH. Images were collected using a ScanAsyst-Air tip (Bruker) operating in "height" mode for topographical images, and in "InPhase" mode for phase images. Raw data images were processed using Gwyddion 2.46 (Open Source software) to obtain useable images.

Organic volume fraction of the imaged particles was determined using both phase and topographical images. In the topographical image, the minimum height occurring in the entire image is set to z = 0, allowing for a reference point which is used later in the calculation (see below).

A mask is applied to the phase image to identify the core of the particle (*SI Appendix* Fig. S12, Part 1A). The core is located using the change in phase lag of the cantilever oscillation referenced to the signal sent to the cantilever, which is represented by a change in the color scale of the phase image. The phase lag results from interaction between the tip and the surface being

imaged, mediated by properties including adhesion, friction, and viscoelasticity as well changes in surface composition (which may also influence the aforementioned properties) (11, 12). Following core identification, the mask of the core is extracted from the image (*SI Appendix* Fig. S12, Part 1B) and translated onto the topographical image of the same particle (*SI Appendix* Fig. S12, Part 1C).

Using the "grain distribution analysis" function in Gwyddion (open source scanning probe microscopy analysis software), the "zero basis volume" for the core mask region of the topographic image is recorded (V_{core}). The zero basis volume, as defined by Gwyddion, is "the volume between the grain surface and the plane z = 0", where here the "grain" is considered the region covered by the core mask. Since the topographical image provides the x, y, and z dimensions of the masked area, whether the height (z) remains constant or varies over the masked area, an accurate volume is attainable (*SI Appendix* Fig. S13) and reported by the zero basis volume value. The masking is then removed and the above steps are repeated for the particle as a whole (see *SI Appendix* Fig. S12, part 2A-C), resulting in a whole particle volume of V_{whole}.

Following this, the V_{whole} and V_{core} are used to calculate the shell volume as V_{whole}-V_{core} = V_{shell}. The assumption here is that complete phase separation has occurred and that the shell contains only organic material while the core contains only inorganic material, which is an assumption commonly made in these types of calculations (13). The organic volume fraction is then determined as V_{shell}/V_{whole}. Additionally, assuming the particles were spherical upon impaction with the substrate allows for calculation of the volume equivalent diameter, $d_{whole} = (3V_{whole})/(4\pi))^{1/3}$.

The height of particle shells were determined from their topographical image, illustrated using a cross-sectional map of height versus x axis position. *SI Appendix* Fig. S14 shows the cross-sectional height profiles of the particles phase-imaged in Figs. 2B and 2D. Two cross-sectional profiles were chosen for the film drop particle and three for the jet drop particle to illustrate the variation in particle height through the core and shell regions. It is evident from both the topographical images and the cross-sectional profiles that the height, and thus thickness, of the particle shell changes in space. However, as explained above, this variability is accounted for in the volume calculation.

Estimate of upper limit of film drop size. A schematic drawing of a floating, sub-100 μm bubble with radius R_b and cap film half angle θ_c is shown in *SI Appendix* Fig. S15. The maximum size of any film drops produced by rupture of the bubble cap can be calculated by assuming the entire cap forms a single film drop. The volume V_c of the cap of a floating bubble is the product of cap thickness, h_b, and area, A_c:

$$V_c = h_b A_c \,, \tag{1}$$

where

$$A_c = 2\pi(1 - \cos(\theta_c))R_b^2 \,,\ \theta_c < \pi/2 \,. \tag{2}$$

Lhuissier and Villermaux (1) found that

$$\theta_c = \frac{R_b}{2\sqrt{3}a} \,, \tag{3}$$

where the capillary number $a = \sqrt{\frac{\sigma}{\rho g}}$, where σ is the surface tension of seawater, ρ is the density of seawater and g is the acceleration due to gravity. Lhuissier and Villermaux find that the cap thickness $h_b \propto R_b^2$, and for R_b = 1 mm, they measured an h_b of 60 nm. Since sub-100 μm bubbles have smaller radii, their cap film heights are also expected to be smaller, but we use h_b = 60 nm to compute an upper limit for the cap film volume. The cap film half angle is calculated using equation (3), yielding a cap film volume of 1.36×10^{-20} m^3 for a bubble of radius 50 μm. If the whole bubble cap only produces one film drop, then the dry diameter for this drop is 74 nm. Most of the electrolysis bubbles were smaller than 50 μm and, even assuming that these bubbles can produce film drops, their dry diameter should be less than 74 nm.

SI FIGURES

Figure S1. Schematic diagram of experimental set-up. **a.** General experimental set-up for SSA particle size/mobility distributions and charge fraction measurement (AMS: aerosol mass spectrometer; DMA: differential mobility analyzer; CPC: condensational particle counter; APS: aerodynamic particle sizer and MART: marine aerosol reference tank). **b.** Electrolysis bubble generation system (MFC: mass flow controller). **c.** Nucleation bubble generator set-up. **d.** Frit chamber set-up. **e.** Experimental set-up for organic volume fraction measurement of film drop and jet drop particles.

a. General experimental set-up for SSA particle size/mobility distributions and charge fraction measurement (AMS: aerosol mass spectrometer; DMA: differential mobility analyzer; CPC: condensational particle counter; APS: aerodynamic particle sizer and MART: marine aerosol reference tank).

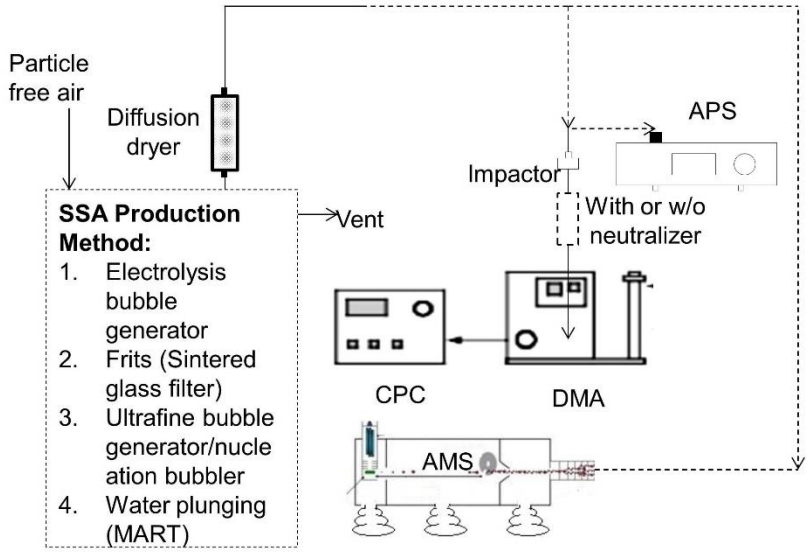

b. Electrolysis bubble generation system (MFC: mass flow controller).

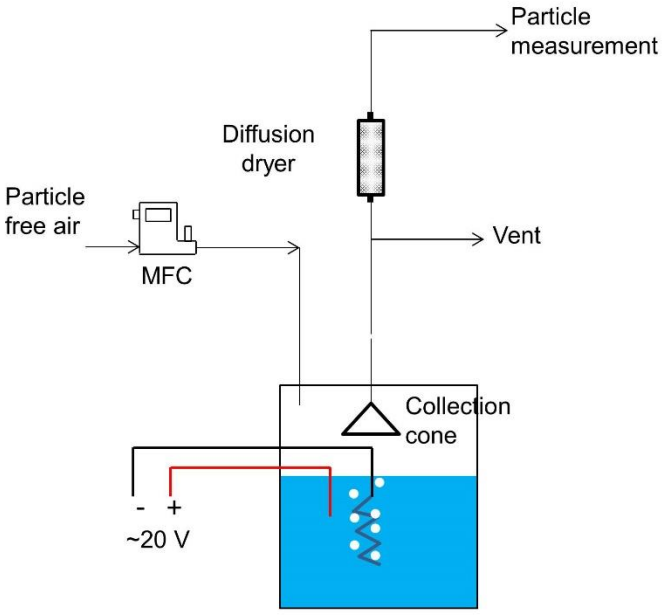

c. Nucleation bubble generator set-up.

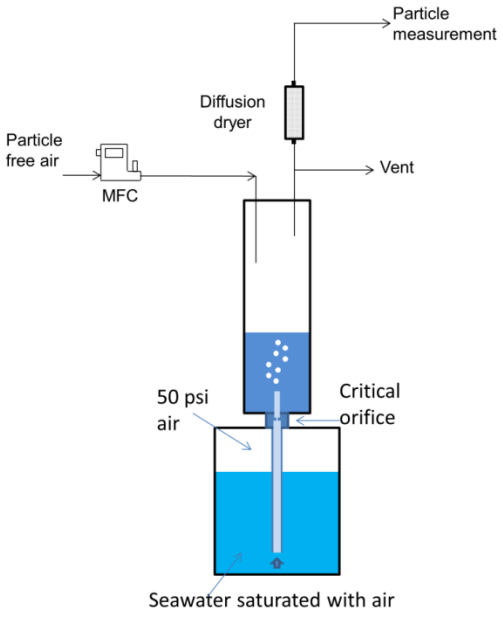

d. Frit chamber set-up.

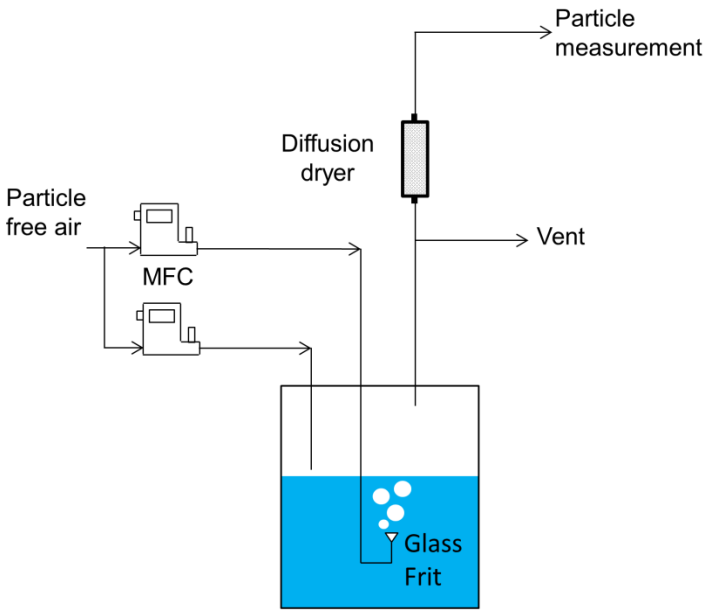

e. Experimental set-up for organic volume fraction measurement of film drop and jet drop particles.

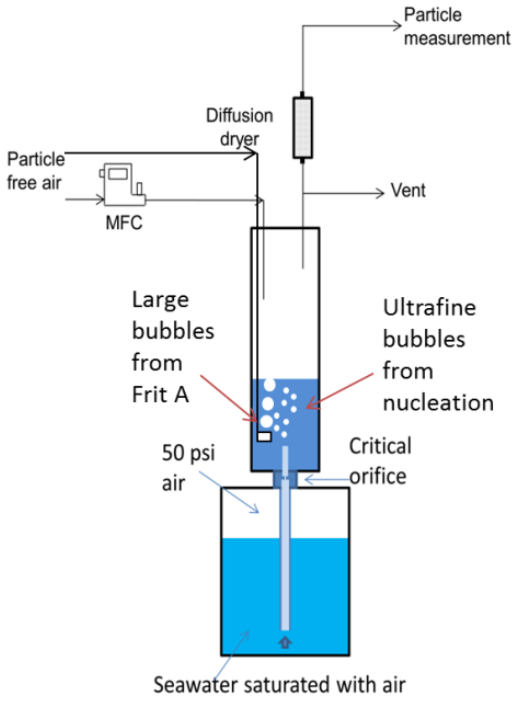

Figure S2. Pictures of sub-100 µm bubble. **a.** Electrolysis bubbles forming on a wire (side view, wire diameter: ~200 µm). **b.** nucleation bubbles (side view).

a.

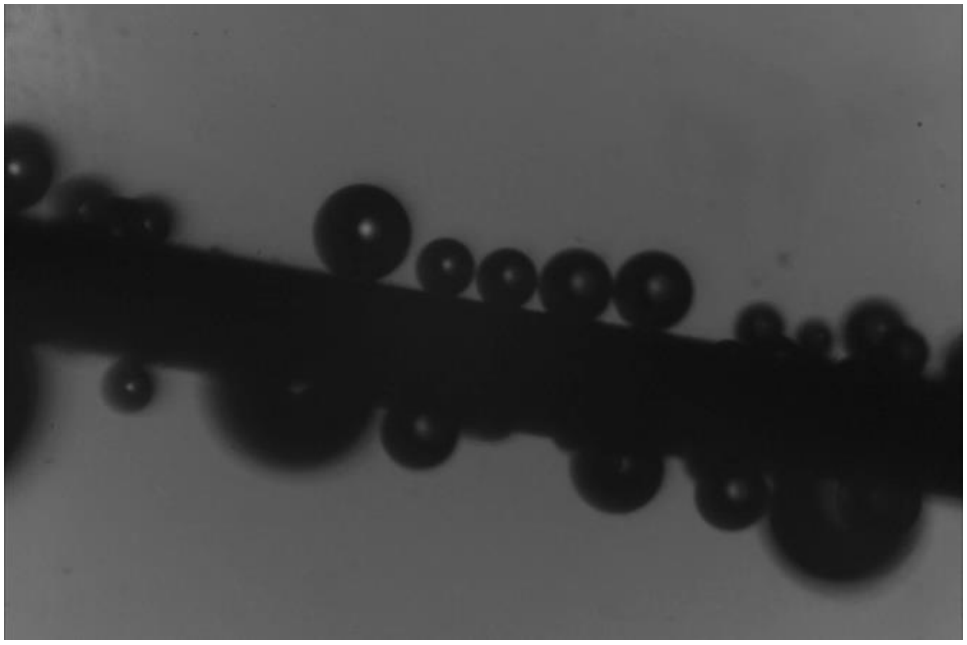

b.

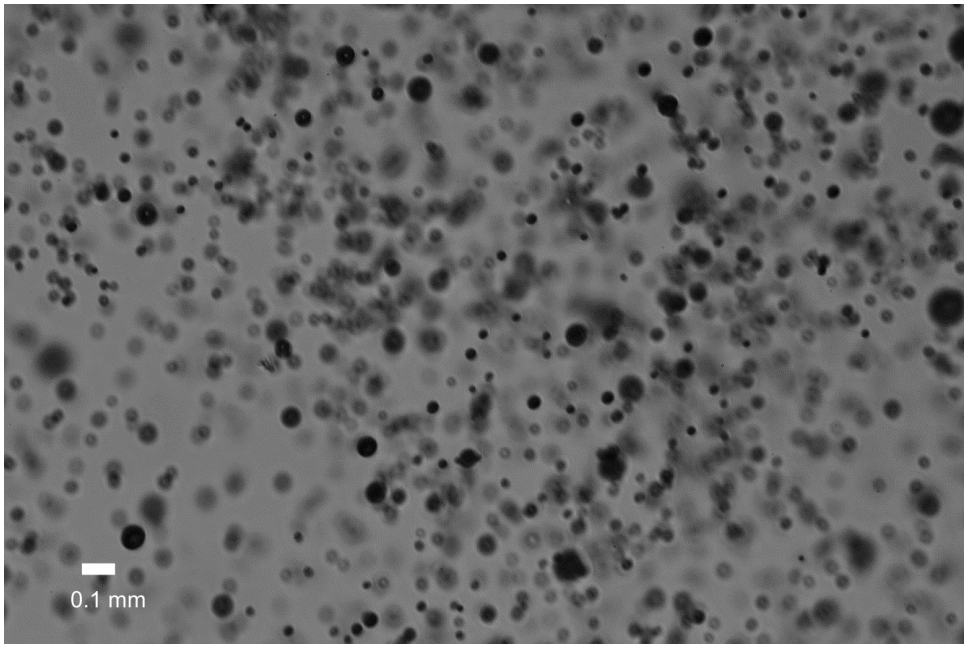

Figure S3. SSA size distribution versus dry diameter for SSA from nucleation bubbles, measured using a scanning mobility particle sizer (SMPS) following an impactor with 800 nm cutoff size. Vertical lines denote standard errors. The inset shows the probability density distribution of nucleation bubble size distribution versus bubble radius in μm.

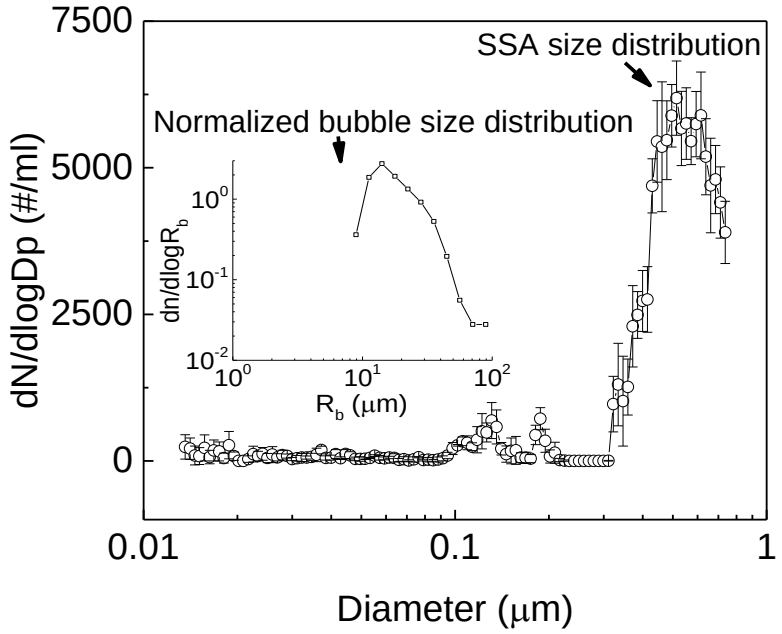

Figure S4. a. Picture of foam and bubbles on the seawater surface in the frit chamber. **b.** Normalized bubble/foam cell size distributions for the frit-sized bubbles. **c.** Particle size distribution for SSA generated from frit-sized bubbles.

a

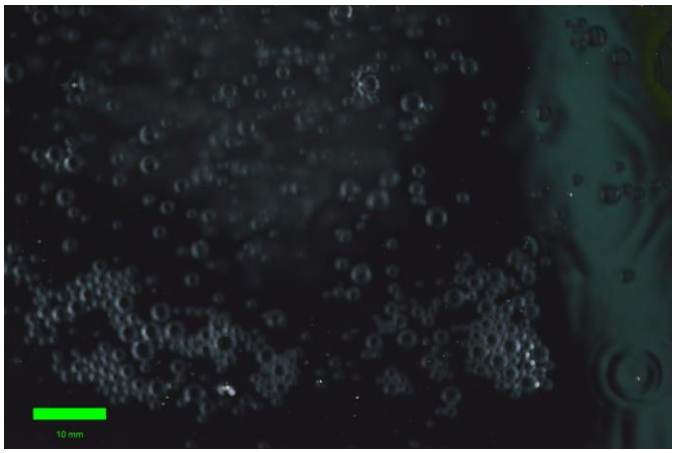

b

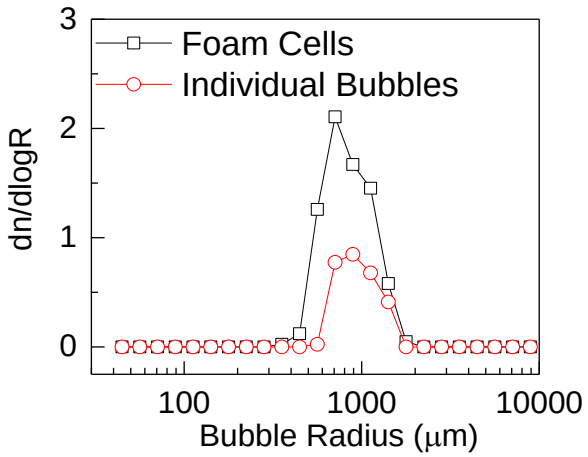

c.

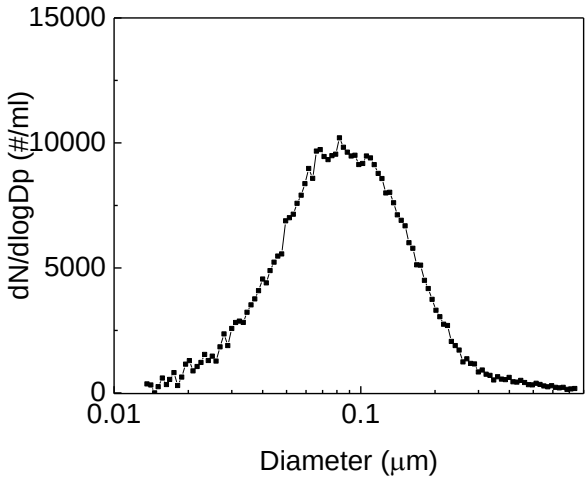

Figure S5. Electrical mobility distributions of submicron SSA particles. **a.** Film drop particles generated with bubbles from the glass frit using (a1) synthetic seawater with low organic content; (a2) real seawater and (a3) real seawater with the addition of 300 µg/L lipids. **b.** Jet drop particles generated from nucleation bubbles using (b1) synthetic seawater with low organic content; (b2) real seawater and (b3) real seawater with the addition of 300 µg/L lipids. The lipids are triglycerides extracted from marine algae. Black squares are EMD^- and red dots are EMD^+. Error bars represent the standard deviation of the data.

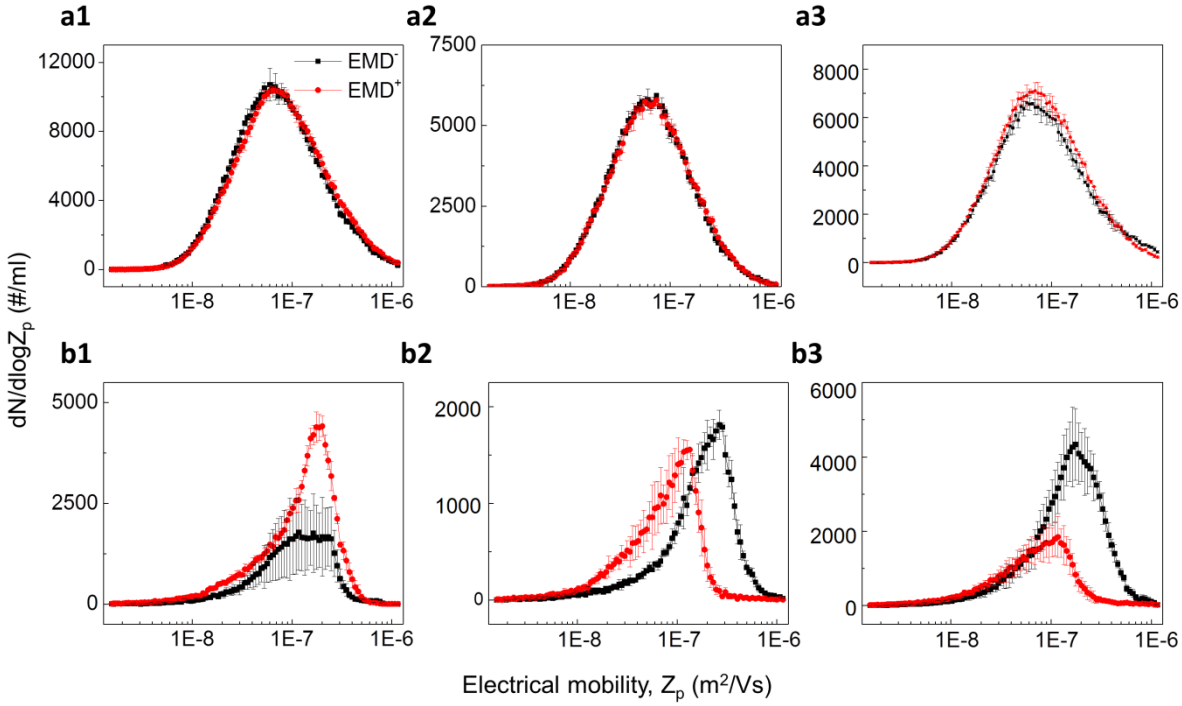

Figure S6. Particle size distribution versus dry diameter for SSA generated using a plunging waterfall in a marine aerosol reference tank (MART).

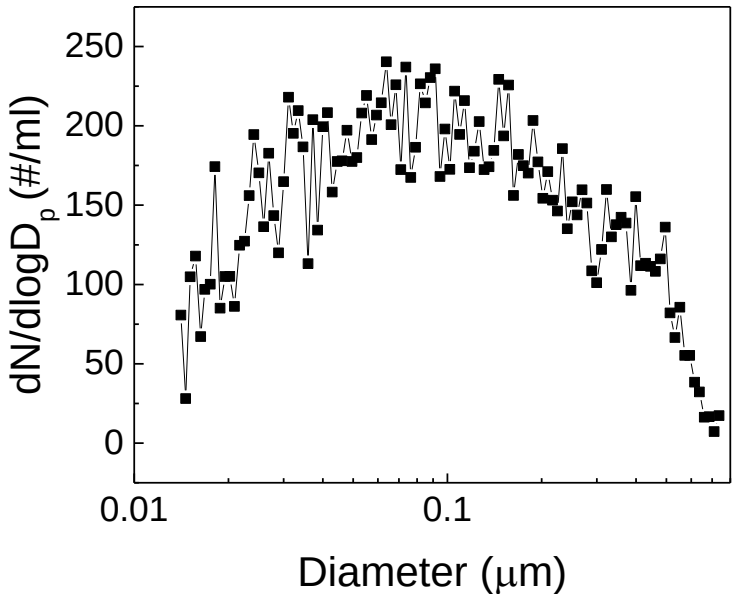

Figure S7. a. Electrical mobility distributions of negatively (EMD^-) and positively (EMD^+) charged submicron SSA produced from water plunging (MART), a realistic SSA production method. The gray lines are fitted results (sum of POS1 + POS2 + POS3 and sum of NEG1 + NEG2 + NEG3). **b.** Three-mode fitting results for the curves (EMD^- and EMD^+) shown in *SI Appendix* Fig. S7a; Error bars represent the standard deviation of the data. The third modes in both EMD^- and EMD^+ (NEG3 and POS3 modes) are much smaller than the four main modes (NEG1, NEG2, POS1 and POS2) and the third mode for fitting the EMD^+ is negative (i.e. non-physical). As with the 2-mode analysis, we can attribute NEG2 and POS2 to jet drop production. The calculated contribution from jet drops is only 1% slightly larger than the result (42%) from 2-mode fitting reported in Fig. 2D.

a.

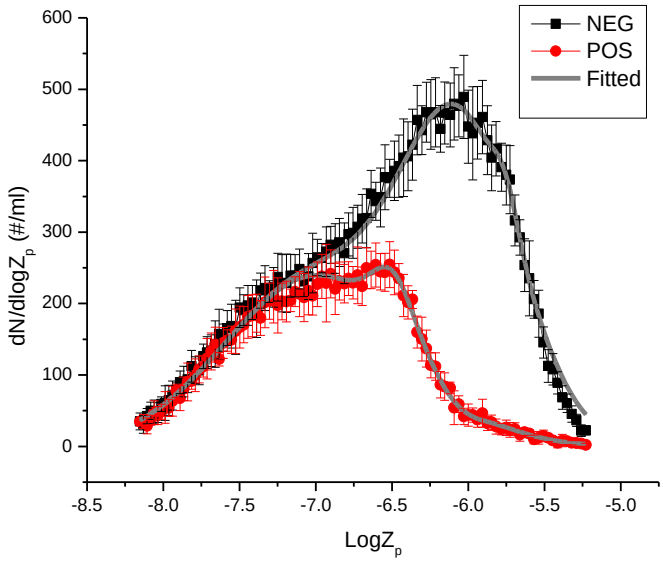

b.

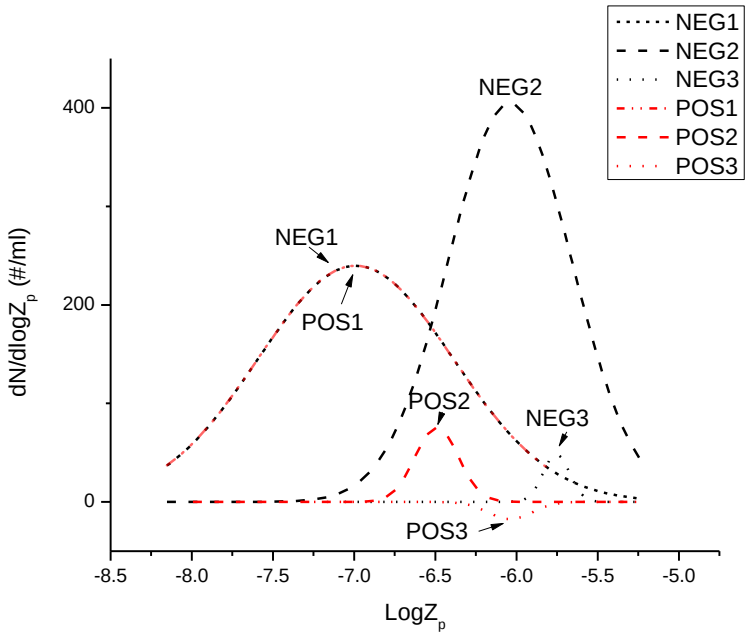
NEG1
NEG2
NEG3
POS1
POS2
POS3
400
200
0
dN/dlogZp (#/ml)
-8.5
-8.0
-7.5
-7.0
-6.5
-6.0
-5.5
-5.0
LogZp

Figure S8. a. Change of chlorophyll-a (chl-a) and total sub-800 nm diameter SSA number concentration during a phytoplankton bloom. **b.** Electrical mobility distributions of submicron SSA measured on successive days during the phytoplankton bloom. Pairs of symbols of the same color show EMD^{+} and EMD^{-} for the same day.

a.

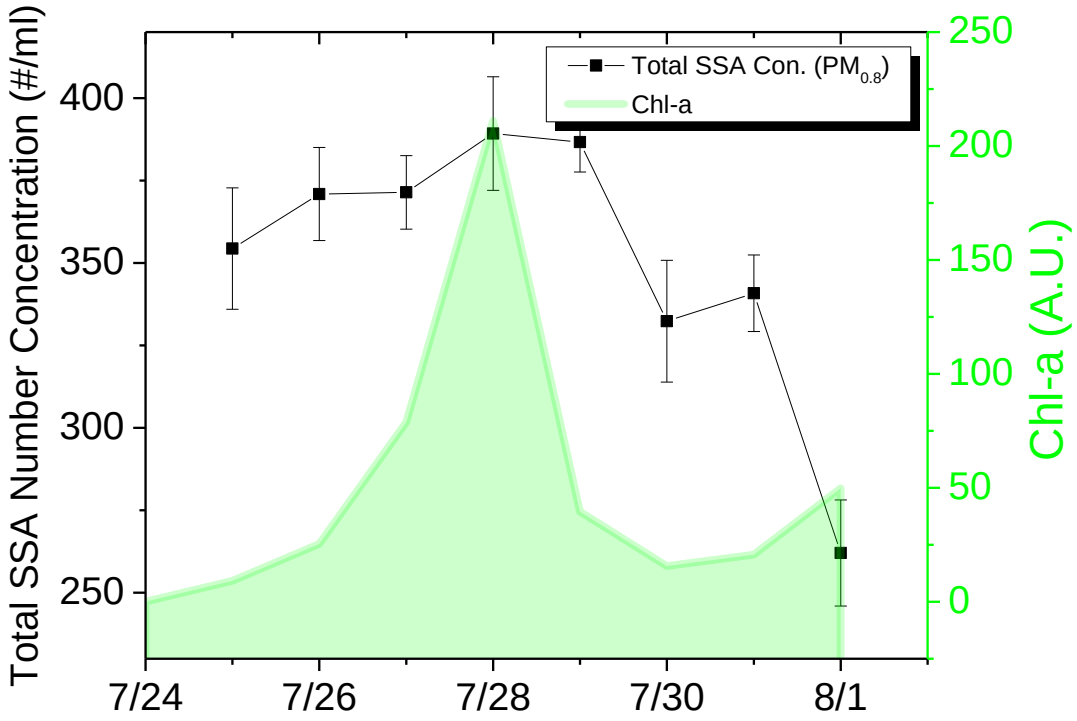

b.

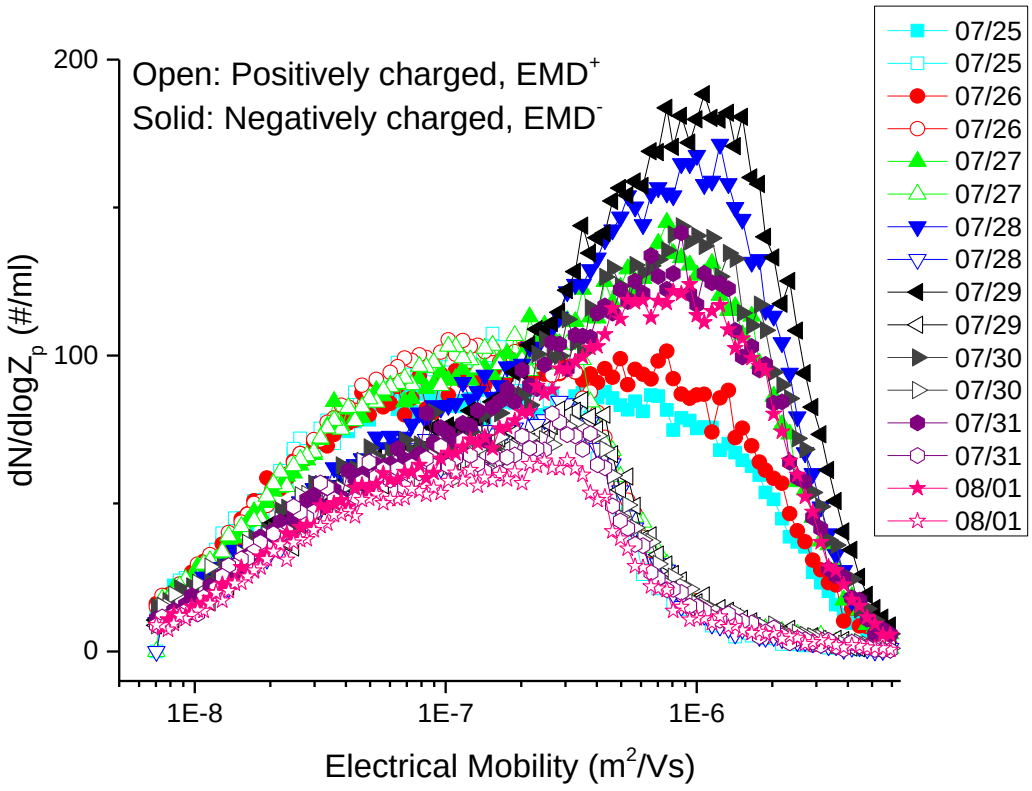
Open: Positively charged, EMD+
Solid: Negatively charged, EMD-
dN/dlogZp (#/ml)
200
100
0
1E-8
1E-7
1E-6
Electrical Mobility (m2/Vs)
07/25
07/25
07/26
07/26
07/27
07/27
07/28
07/28
07/29
07/29
07/30
07/30
07/31
07/31
08/01
08/01

Figure S9. Time series of number concentrations of film drop particles and jet drop particles measured during the phytoplankton bloom. See main text for the method of calculation.

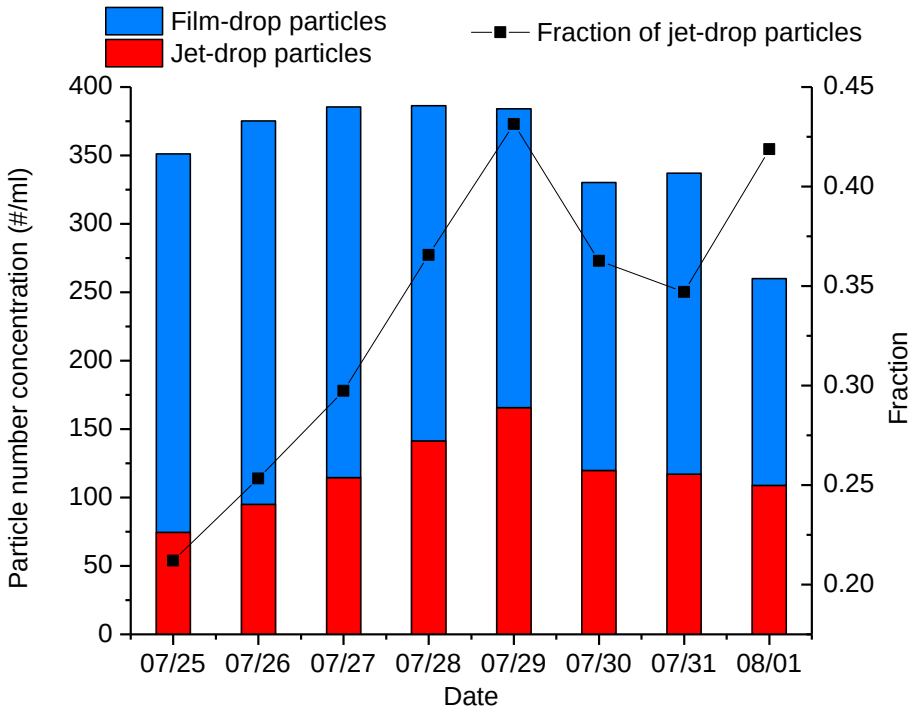

Figure S10. Size distribution of a mixture of submicron film drop and jet drop particles versus dry diameter. Particles were produced by bursting large and sub-100 μm bubbles together in the experiment set-up shown in *SI Appendix* Fig. S1E.

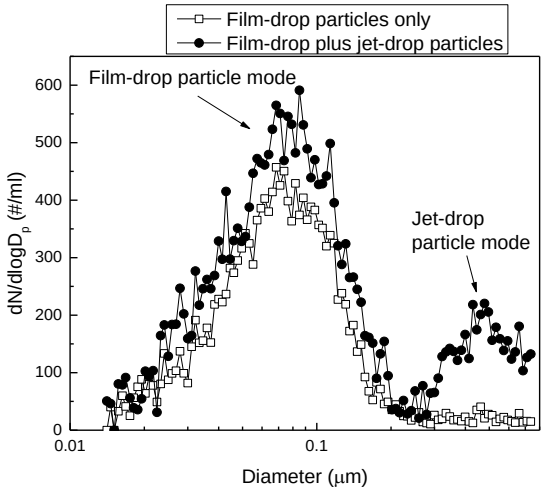

Figure S11. Number fraction of INPs in submicron SSA from film and jet drops. The data points are reproduced from Fig. 2F. The black and blue lines respectively are exponential fits to the film drop and jet drop curves. The particle size distributions (*SI Appendix* Fig. S3 and S4) can be used to calculate average volume and surface area per particle. The average volumes for the film drop and jet drop particle are 0.0023 and 0.082 μm^3, respectively, while the average surface areas for the film drop and jet drop particle are 0.053 and 0.85 μm^2 respectively. The purple line is the fitted film drop curve multiplied by a factor of (0.082/0.0023) = ~36, which represents volume scaling. The green line is the fitted film drop curve multiplied by a factor of (0.85/0.053) = ~16, which represents surface area scaling.

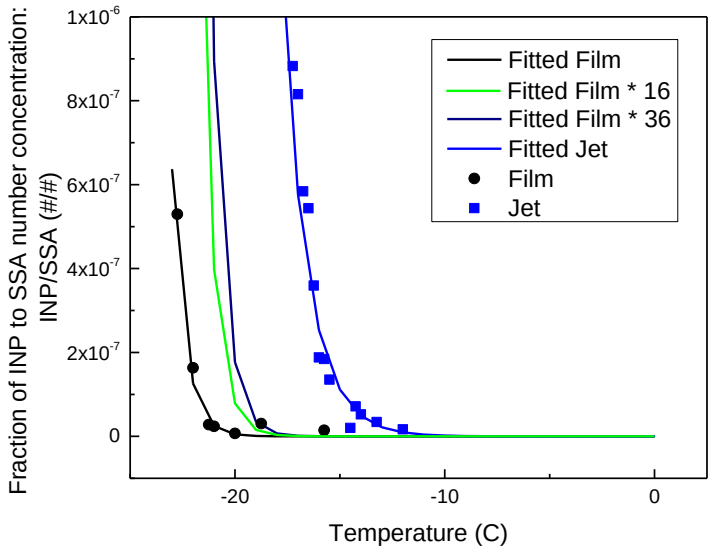

Figure S12. AFM images of SSA particles. Part 1 illustrates the results of the image processing steps involved in calculating the volume of each individual particle core. Part 2 illustrates the results of the image processing steps involved in calculating each particle volume as a whole.

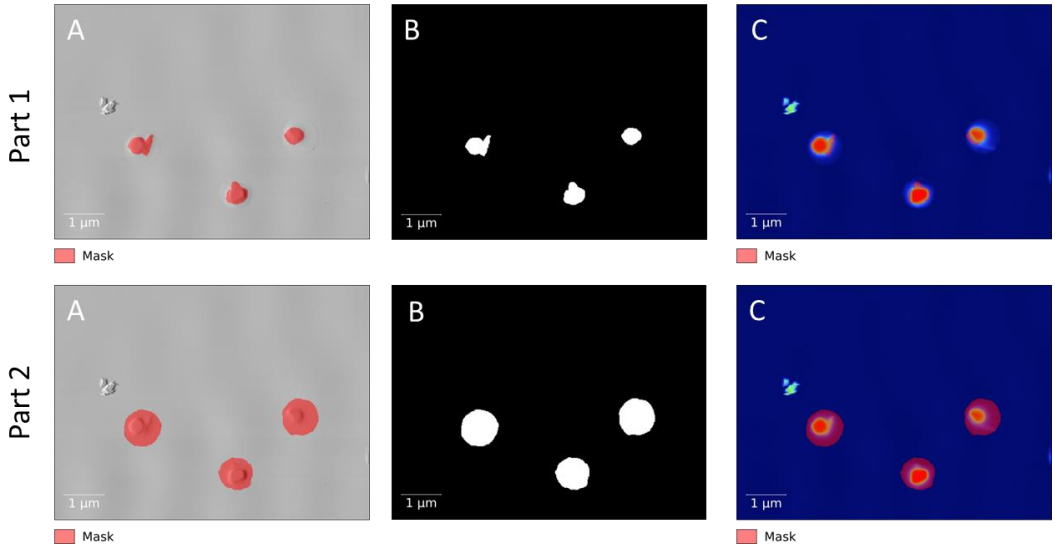

Figure S13. A three dimensional view of the topographical image used in *SI Appendix* Fig. S12 (no mask is shown or applied here), illustrating the measured x, y, and z dimensions of non-axisymmetric particles (the total length of x-edge is 8 μm and the total length of y-edge is 6 μm).

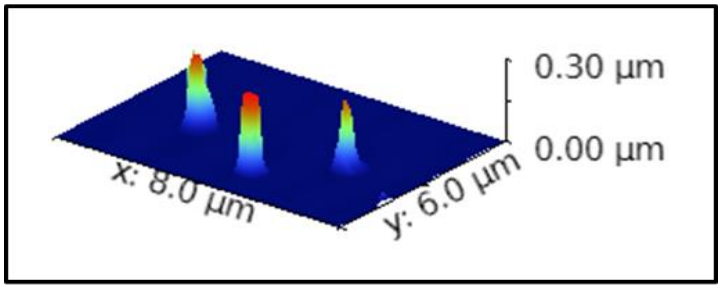

Figure S14. Selected profiles of particle height. **First column**: height image of the representative film drop particle shown in Fig. 3B. A height profile through the cross-section of the particle core (green line) is shown in Panel A, and across the shell (red line) is shown in Panel B. **Second column**: as for first column, but for the jet drop particle shown in Fig 3D. A height profile through the cross-section of the particle core (green line) is shown in Panel A. Panel B shows height profiles across two sections of the shell (red and yellow lines).

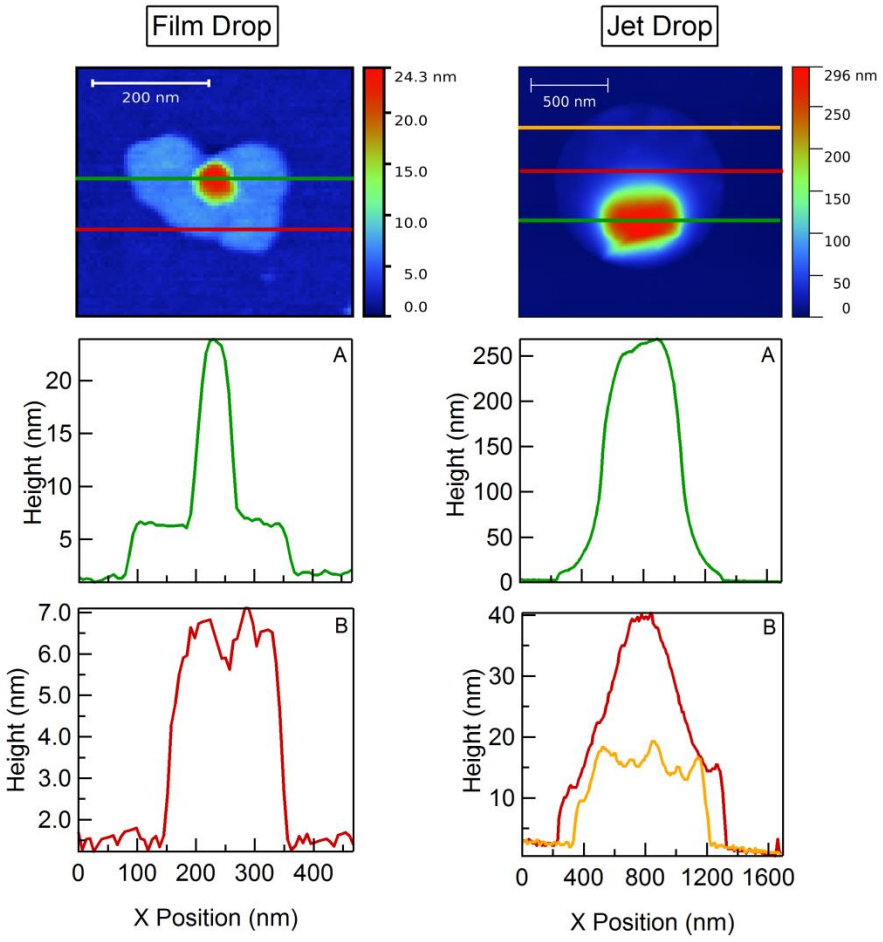

Figure S15. Schematic drawing of a floating bubble.

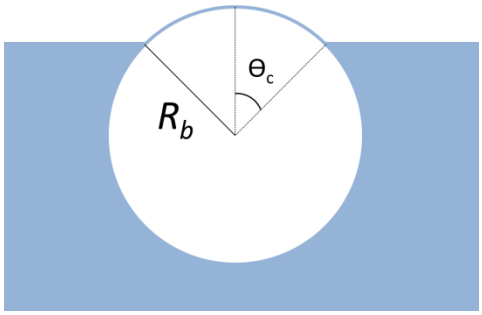

REFERENCES:

1. Lhuissier H & Villermaux E (2012) Bursting bubble aerosols. *J Fluid Mech* 696:5-44.

2. Lee JS, *et al.* (2011) Size limits the formation of liquid jets during bubble bursting. *Nat Commun* 2:367.

3. Lee C, *et al.* (2015) Advancing model systems for fundamental laboratory studies of sea spray aerosol using the microbial loop. *J Phys Chem A* 119(33):8860-8870.

4. Stokes MD, *et al.* (2013) A marine aerosol reference tank system as a breaking wave analogue for the production of foam and sea-spray aerosols. *Atmos Meas Tech* 6(4):1085-1094.

5. Buckley AJ, Wright MD, & Henshaw DL (2008) A technique for rapid estimation of the charge distribution of submicron aerosols under atmospheric conditions. *Aerosol Sci Technol* 42(12):1042-1051.

6. DeCarlo PF, *et al.* (2006) Field-deployable, high-resolution, time-of-flight aerosol mass spectrometer. *Anal Chem* 78(24):8281-8289.

7. Canagaratna MR, *et al.* (2015) Elemental ratio measurements of organic compounds using aerosol mass spectrometry: characterization, improved calibration, and implications. *Atmos Chem Phys* 15(1):253-272.

8. Burrows SM, *et al.* (2014) A physically based framework for modeling the organic fractionation of sea spray aerosol from bubble film Langmuir equilibria. *Atmos Chem Phys* 14(24):13601-13629.

9. Wang XF, *et al.* (2015) Microbial control of sea spray aerosol composition: a tale of two blooms. *ACS Central Sci* 1(3):124-131.

10. Agresti A & Coull BA (1998) Approximate is better than "exact" for interval estimation of binomial proportions. *Am Stat* 52(2):119-126.

11. Magonov, SN, *et al.* (1997), Phase imaging and stiffness in tapping-mode atomic force microscopy, *Surf Sci* 375(2): L385-L391.

12. Pang, GK, *et al.* (2000), Topographic and phase-contrast imaging in atomic force microscopy, *Ultramicroscopy*, *81*(2), 35-40.

13. Ryder, OS, *et al.* (2014), On the role of particle inorganic mixing state in the reactive uptake of N2O5 to ambient aerosol particles, *Environ Sci Technol*, *48*(3), 1618-1627.